APPLIED ORGANOMETALLIC CHEMISTRY, VOL. 5, 247–255 (1991)

Laser photodissociation of organometallic compounds on a cryosubstrate

Masahiro Kawasaki* and Nobuyuki Nishi†
*Research Institute of Applied Electricity, Hokkaido University, N12W6, Sapporo 060, Japan, and
†Institute for Molecular Science, Myodaiji, Okazaki 444, Japan

The photodissociation dynamics of organometallic compounds (tetramethyltin, trimethylgallium, trimethylindium and dimethylzinc) adsorbed on a quartz substrate at 100 K have been studied by time-of-flight mass spectrometry, detecting mainly CH_3 photofragments. Shapes of the time-of-flight spectra depend on the flux of the dissociation laser at 193 nm and the thickness of multilayers of organometallic compounds. In thick layers, not only a low energy component but also a high energy component are observed in the time-of-flight spectrum of the CH_3 photofragments. In thin layers, relaxation processes take place so quickly that the product time-of-flight profiles are characterized by a Maxwell–Boltzmann temperature profile.

Keywords: Photodissociation, organometallic, time-of-flight, translational energy, dynamics, photoejection, excimer laser

1 INTRODUCTION

Laser surface chemistry has been used as a basis for many new techniques in surface processing, including photochemical vapor deposition of metals, semiconductors and insulators, which are potentially useful for the microelectronics industry.[1–4] Analytical efforts to study the laser photolysis of adsorbate systems are only just beginning: spectroscopic techniques used recently for surface photochemistry are time-of-flight (TOF) mass spectroscopy,[5–11] time-resolved laser-induced fluorescence,[12,13] *in situ* ESCA[14] and UV spectroscopy.[15]

The irradiation by photons of organic and inorganic compounds adsorbed on substrates leads to a nonthermal photochemistry that is different from that observed in the gas phase. Photodissociation of monolayers on substrates has been reported by some groups. They have measured the translational energy distribution of photofragments from monolayers of chlorine Cl_2,[8] H_2S,[6,7] CH_3Cl,[8] CH_3Br,[6,7] trimethylaluminum $Al(CH_3)$,[10] dimethylzinc $Zn(CH_3)_2$,[11] trimethylgallium $(Ga(CH_3)_2)$ and trimethylindium $(In(CH_3)_3)$[12,13] ejected from the substrates. The dynamics of the surface photodissociation processes were found to vary with the coverage of the adsorbed layers.[6–9] In general, for higher coverage, both slow and fast photofragments are ejected from the substrate by laser irradiation whilst for lower coverage only slow photofragments are observed.[11]

In the photodissociation of trimethylgallium on a substrate at room temperature, gallium atoms are detected by laser-induced fluorescence[12,13] whilst aluminum atoms are not detected by a time-of-flight technique.[10] Higashi[10] has stated that the absence of aluminum signal is particularly significant because this substantiates the view that aluminum atoms are strongly bound to the surface. In the gas phase, organometallic compounds strongly absorb UV photons at <200 nm,[16] resulting in the formation of methyl radicals and other fragments. For example, the photodissociation of gaseous tetramethyltin at 193 nm has been reported.[17] Photoexcited molecules dissociate into both $Sn(CH_3)_3 + CH_3$ and $Sn(CH_3)_2 + 2CH_3$ by two-body and three-body dissociation processes, respectively. $Cd(CH_3)_2$ and $Zn(CH_3)_2$ form electronically excited CH_3Cd and CH_3Zn radicals by 193 nm irradiation in the gas phase.[18] In order to understand how the nature of photon–adsorbate interactions change in different environments, we investigated the UV photodissociation of monolayers and multilayers of molecules on a cryosubstrate.

2 EXPERIMENTAL

The experimental apparatus[19] is drawn schematically in Fig. 1. The reaction and detector chambers are differentially pumped by turbomolecular pumps and a diffusion pump. The pressures of these chambers were 10^{-9} and 10^{-10} Torr,

0268-2605/91/040247-09$05.00

Received 18 February 1991
Accepted 13 April 1991

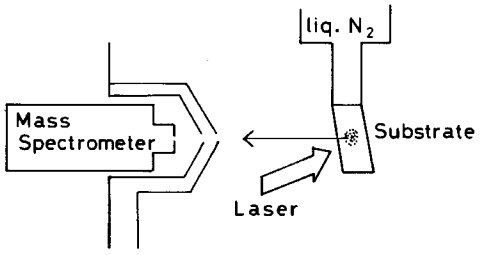

Figure 1 Schematic diagram of the experimental set-up for solid photolysis. The hollow arrow indicates the laser beam.[19]

respectively. The quartz substrate is cooled to 100 K by a liquid nitrogen trap, on which the sample molecules, dimethylzinc ($Zn(CH_3)_2$), trimethylindium ($In(CH_3)_3$), trimethylgallium ($Ga(CH_3)_3$) or tetramethyltin ($Sn(CH_3)_4$), are deposited through a capillary tube until they form multilayers on the substrate. An ArF excimer laser (193 nm) is used to irradiate the molecules on the substrate at glancing incidence (80° to the normal) with unpolarized radiation. The laser power used is 50–100 mJ cm^{-2}.

Radicals ejected from the substrate were detected by a quadrupole mass spectrometer with an electron-bombardment ionizer under conditions of electron energy = 44 V for the $Sn(CH_3)_4$ experiment and 20 eV for other compounds, ion energy = 20 V as a function of mass numbers and time after laser pulses. The flight length was 16 cm.

High-purity sample gases $Zn(CH_3)_2$, $In(CH_3)_3$ and $Ga(CH_3)_3$ were supplied by Sumitomo Chemical Co. Research-grade $Sn(CH_3)_4$ was purchased from Wako Chemicals.

3 RESULTS

3.1 Photodissociation of tetramethyltin at 193 mm

3.1.1 Time-of-flight distribution of photofragments

The laser-irradiated $Sn(CH_3)_4$ molecules were deposited on the quartz plate cooled to 100 K. Photofragments were detected by the mass spectrometer with an electron bombardment ionizer. Detected ions were CH_3^+ and $Sn(CH_3)_m^+$ ($m = 0$–4). Some of these ions were generated in the ionizer by dissociative ionization of neutral photofragments or parent molecules desorbed. The TOF spectra of these species were measured as shown in Figs 2 and 3. Both the threshold and

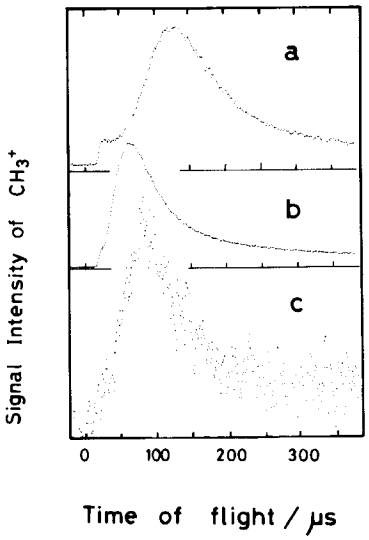

Figure 2 Time-of-flight spectra of CH_3 radicals obtained in $Sn(CH_3)_4$ photolysis at 193 nm on the quartz substrate cooled at 100 K and in the gas phase. (a) Low laser energy flux (50 mJ cm^{-2}); (b) high laser energy flux (100 mJ cm^{-2}); (c) gas-phase photolysis.

peak TOF signals obtained from these figures are summarized in Table 1.

A comparison of the time-of-flight profile of the CH_3^+ signal (Fig. 2) with that of the $Sn(CH_3)_m^+$ signal (Fig. 3) reveals that the CH_3^+ ion does originate neither from the dissociative ionization of parent molecules nor from tin-containing photofragments, but rather by low-energy (44 V) electron bombardment ionization of CH_3 photofragments. This was also reported in the multiphotoionization and low-energy (30 V) electron bombardment of CH_3 fragments produced from

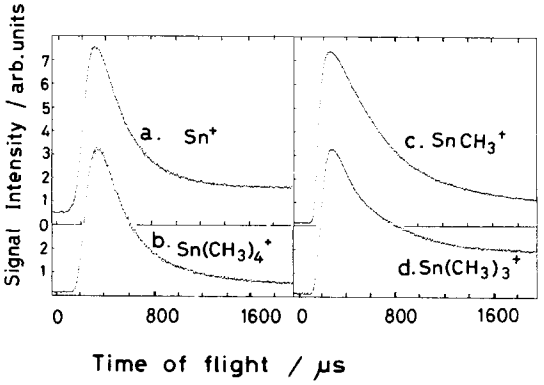

Figure 3 Time-of-flight spectra of $Sn(CH_3)_m^+$ obtained in photolysis of solid $Sn(CH_3)_4$ at 193 nm on the quartz substrate cooled at 100 K. Detected ions are (a) Sn^+; (b) $Sn(CH_3)_4^+$; (c)$SnCH_3^+$; (d) $Sn(CH_3)_3^+$.

Table 1 Time-of-flight results and average energies of photofragments from the photodissocaition of organometallic compounds at 193 nm on cryosubstrate at 100 K

Parent Molecule	Detected Species (amu)	t_{TH}[a] (μs)	t_p[b] (μs)	$\bar{E}_{T_1}$[c] kJ mol^{-1})	$\bar{E}_{T_2}$[c]
$Sn(CH_3)_4$	CH_3^+ (15)	23 ± 2	33/68	2.1	42
	Sn^+ (120)	150 ± 5	330	1.7	21
	$SnCH_3^+$ (135)	114 ± 10	250	7.1	37.8
	$Sn(CH_3)_3^+$ (165)	120 ± 10	250	2.1	29.4
	$Sn(CH_3)_4^+$ (180)	140 ± 5	310	0.8	25.2
$In(CH_3)_3$	CH_3^+ (15)	25 ± 2	70/270	2.9	37.8
$Ga(CH_3)_3$	CH_3^+ (15)	—	60/130/220	—	—
$Zn(CH_3)_2$	CH_3^+ (15)	29 ± 2	60/210	3.4	21
	CH_3^+ (15)[d]	~100	~180	7.1	—

[a] Threshold appearance time-of-flight. [b] Peaked time-of-flight. [c] Assuming bimodal Maxwell–Boltzmann distributions of Eqn [6], $\bar{E}_{T_i} = (3/2)k_{T_i}$. [d] Experiment on a room temperature substrate.

the photodissociation of solid $Zn(CH_3)_2$ by Howitz *et al.*[11] Figure 2(a) and (b) shows the laser power dependence of the TOF shapes of the CH_3^+ photofragments. For Fig. 2(b) the laser energy flux is twice as large as for Fig. 2(a). At the high laser energy flux the TOF spectrum shifts toward the faster region, peaking at 70 μs. At low flux it peaks at 130 μs. For purposes of comparison, the result of the gas-phase photodissociation of a $Sn(CH_3)_4$ molecular beam is shown in Fig. 2(c), which was measured previously with the same spectrometer that was used for this study.[17] Figure 2(c) shows that the TOF of CH_3^+ peaks at 80 μs in the molecular beam experiment, which is close to that obtained in Fig. 2(b). At high energy flux, parent molecules may be desorbed from the solid by laser irradiation, resulting in gas-phase photodissociation during the laser pulse duration of 15 ns, viz.

$$(Sn(CH_3)_4)_{solid} + h\nu \rightarrow (Sn(CH_3)_4)_{vapor} \quad [1]$$

$$(Sn(CH_3)_4)_{vapor} + h\nu \rightarrow CH_3^+ \ldots \quad [2]$$

Hence, the strong and slow peak observed at TOF = 130 μs in Fig. 2(a) is not due to gas-phase photodissociation but to photodissociation of solid $Sn(CH_3)_4$.

The fast weak peak of Figs 2(a) and (b) starts to appear at 23 μs and shows a hump at 33 μs. If these signals are due to the solid-phase photodissociation of $Sn(CH_3)_4$, the fastest CH_3^+ radicals can carry all the excess energy, $E_{ex} = h\nu - D_0$, as translational energy because the substrate carries no translational energy. The threshold TOF of 23 ± 2 μs corresponds to $360 \pm \frac{80}{50}$ kJ mol^{-1}, in good agreement with that calculated with $h\nu$ = 619 kJ mol^{-1} and $D_0 = 250 \pm 10$ kJ mol^{-1}.

We must consider the fact that $Sn(CH_3)_m^+$ ($m = 0$–3) can be generated by dissociative ionization processes in the ionizer. The parent molecule is promptly photodesorbed by UV laser irradiation. The strong Sn^+ signals are produced by dissociative ionization of $Sn(CH_3)_4$ because (i) the TOF shape of Sn^+ in Fig. 3(a) resembles that of $Sn(CH_3)_4^+$ in Fig. 3(b) and (ii) the threshold TOF of Sn^+(150 ± 5 μs) is in agreement with that of $Sn(CH_4)_4^+$ (140 ± 5 μs). Similarly, the most probable source of $SnCH_3^+$ is dissociative ionization of $Sn(CH_3)_3^+$, because (i) the shape of Fig. 3(c) resembles that of Fig. 3(d) and (ii) the threshold TOF of 114 ± 10 μs for $SnCH_3^+$ is in agreement with 120 ± 10 μs for $Sn(CH_3)_3^+$. However, when one compares carefully the TOF spectra of $Sn(CH_3)_3^+$ with the spectrum of $SnCH_3^+$ one finds that the $Sn(CH_3)_3^+$ signals are stronger in intensity at TOF > 600 μs than the $SnCH_3^+$ signal. Part of this $Sn(CH_3)_3^+$ signal must be generated by the dissociative ionization of the parent molecules that are desorbed by laser irradiation. Hence, the true TOF spectrum for $Sn(CH_3)_3$ neutral photofragments is represented by that of $SnCH_3^+$ and not by that of $Sn(CH_3)_3^+$.

3.1.2. Translational energy distribution of photofragments

The TOF spectra of the photofragments are converted to a translational energy distribution $P(E_T)$ with a suitable Jacobian factor.[19] For the CH_3^+ photofragments, the energy distribution is obtained at a laser flux of 50 mJ cm^{-2} (Fig. 4(a)),

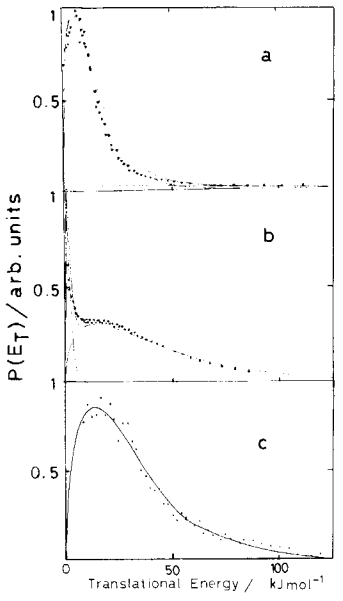

Figure 4 Translational energy distributions, $P(E_T)$, of CH_3 radicals obtained in solid and gas photodissociation of $Sn(CH_3)_4$ at 193 nm. Dotted data are from Fig. 2. Solid lines are simulated curves from Eqn [6] with parameters from Table 1. (a) Low laser energy flux (50 mJ cm^{-2}); (b) high laser energy flux (100 mJ cm^{-2}; (c) gas-phase photolysis.

100 mJ cm^{-2} (Fig. 4(b)), or for the gas phase photodissociation (Fig. 4(c)). At 50 mJ cm^{-2} the translational energy distribution peaks at 8.4 kJ mol^{-1} while at 100 mJ cm^{-2} and for the gas-phase photodissociation, the distribution of CH_3 peaks at 17 kJ mol^{-1}. As mentioned above, at high laser energy flux, the parent $Sn(CH_3)_4$ molecules photodesorbed by laser irradiation undergo photodissociation near the substrate. The energy distribution of Fig. 4(b) which peaks at 17 kJ mol^{-1} resembles that of the gas-phase photolysis of Fig. 4(c). Hence, the distribution of Fig. 4(a), i.e. the low-flux case, shows the nascent distribution of CH_3 radicals produced from the photodissociation of solid $Sn(CH_3)_4$. In the solid-phase dissociation, $P(E_T)$ peaks at low kinetic energy. This component is characteristic of a fast relaxation process in the solid photolysis.

The TOF signals of the parent ions $Sn(CH_3)_4^+$ are converted to the translational energy distribution of photodesorbed $Sn(CH_3)_4$ as shown in Fig. 5(a). However, a part of the $Sn(CH_3)_3^+$ signals were generated by dissociative ionization of $Sn(CH_3)_4$ in the ionizer; the TOF distribution of $Sn(CH_3)_3^+$ is not analyzed. Instead, the $SnCH_3^+$ signal was converted to $P(E_T)$ as the translational energy distribution of $Sn(CH_3)_3$. The result is shown in Fig. 5(b). There seem to be two energy distributions; one peaks near zero and the other at ~10 kJ mol^{-1}. The average translational energies will be discussed below.

3.2 Photodissociation of trimethylindium at 193 nm

$In(CH_3)_3$ deposited on a quartz substrate cooled to 100 K was irradiated with 193 nm laser light. CH_3^+ ions were detected by the mass spectrometer as shown in Fig. 6. As stated above, CH_3^+ signals originate from CH_3 photofragments under the experimental conditions of low electron energy for ionization (20 V). Hence, Fig. 6 gives the TOF spectrum of the CH_3 photofragments from solid $In(CH_3)_3$. Both a fast and a slow signal peaks are observed. The threshold TOF is observed at 25 ± 2 μs and the peak TOF signal is at 70 ± 5 μs for the fast component and at 270 ± 5 μs for the slow one. This bimodal distribution is typical in photodissociation of solid molecules, as is observed in Fig. 2(a). The TOF spectrum of this CH_3 radical is converted to the translational energy distribution as given in Fig. 7. One peaks at low translational energy and the other at ~10 kJ mol^{-1}. Average translational energies are 3 and 38 kJ mol^{-1} assuming a Maxwell distribution for the velocities.

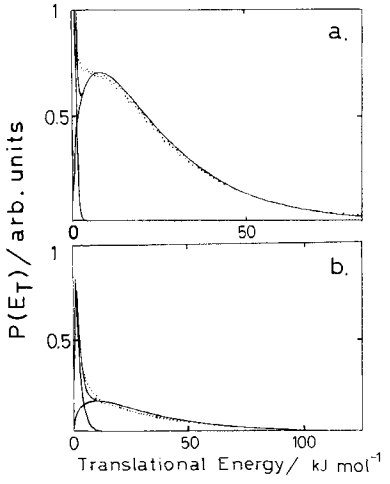

Figure 5 Translational energy distributions $P(E_T)$ of $Sn(CH_3)_4$ parent molecules (a) and $Sn(CH_3)_3$ radicals (b) obtained in laser irradiation of solid $Sn(CH_3)_4$ at 193 nm. $Sn(CH_3)_4$ signals are observed as $Sn(CH_3)_4^+$ whilst $Sn(CH)_3$ signals are observed as $SnCH_3^+$ by dissociative ionization in the ionizer. Solid lines are simulated $P(E_T)$ from Eqn [6] with parameters from Table 1.

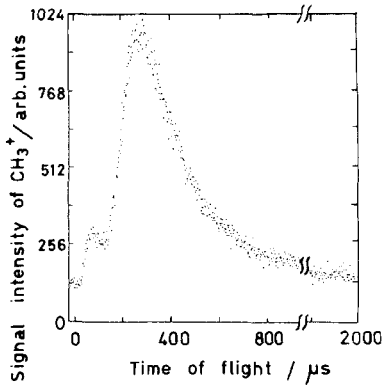

Figure 6 Time-of-flight spectrum of CH_3 radicals obtained in solid $In(CH_3)_3$ photodissociation at 193 nm on the quartz substrate cooled at 100 K. The detected species is CH_3^+.

3.3 Photodissociation of trimethylgallium at 193 nm

The TOF spectrum of CH_3^+ signals from photodissociation of solid $Ga(CH_3)_3$ (Fig. 8) shows a rather complicated shape. TOF spectrum peaks at 60 μs, 130 μs, and 220 μs are marked by arrows in Fig. 8. This may be compared with the photodissociation of $Sn(CH_3)_4$ and $In(CH_3)_2$ which have only two peaks (Figs 2 and 6). This fact may reflect a rather complicated dissociation process for solid $Ga(CH_3)_3$.

3.4 Photodissociation of dimethylzinc at 193 nm

$Zn(CH_3)_2$ deposited on the quartz substrate cooled to 100 K was irradiated with a laser beam. The CH_3^+ signals show a bimodal distribution, as in Fig. 9(a). The threshold TOF is 29 ± 2 μs. TOF

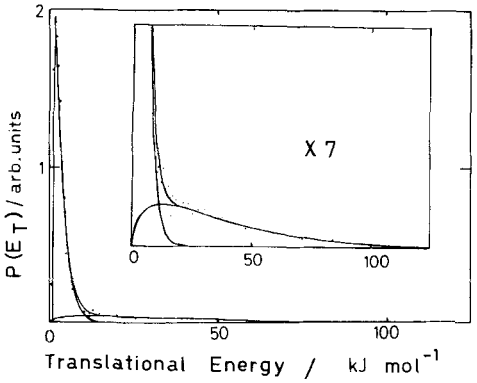

Figure 7 Translational energy distribution of CH_3 radicals obtained in photodissociation of solid $In(CH_3)_3$ at 193 nm. The solid lines are simulated curves from Eqn [6] with parameters from Table 1.

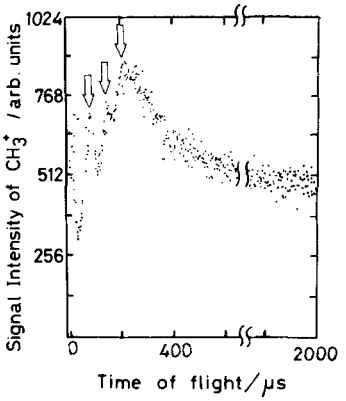

Figure 8 TOF spectrum of CH_3 radicals obtained in photolysis of solid $Ga(CH_3)_3$ at 193 nm on the quartz substrate cooled at 100 K. The arrows show the positions of peaks in the spectrum.

peaks are at 60 and 210 μs as summarized in Table 1. When the substrate was warmed up to room temperature, $Zn(CH_3)_2$ was desorbed, leaving a monolayer of $Zn(CH_3)_2$ on the substrate. Laser irradiation of this substrate gave CH_3 signals as shown in Fig. 9(b), peaking at 180 μs. This peak position is close to the slow one observed at 210 μs in the photodissociation of solid $Zn(CH_3)_2$ shown in Fig. 9(a).

These TOF spectra are converted to $P(E_T)$ as shown in Fig. 10. There seem to be two different energy distributions in Fig. 10(a) for the solid photodissociation, while only the low-energy component appears in Fig. 10(b) for dissociation of the monolayer.

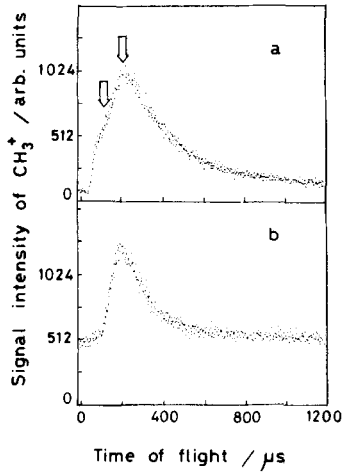

Figure 9 TOF spectrum of CH_3 radicals obtained in $Zn(CH_3)_2$ photodissociation at 193 nm (a) on a quartz substrate cooled at 100 K, and (b) on a quartz substrate at 300 K.

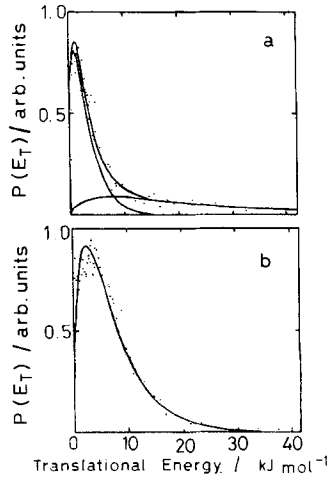

Figure 10 Translational energy distribution of $CH_3^{\cdot}$ radicals obtained in photodissociation of solid $Zn(CH_3)_2$ at 193 nm. The solid lines are simulated curves from Eqn [6] with parameters from Table 1. (a) Solid photodissociation on a quartz substrate cooled to 100 K; (b) monolayer photodissociation on a quartz substrate at room temperature.

4 DISCUSSION

4.1 Effect of thickness of multilayers of organometallic compounds on TOF distributions

As mentioned in Section 3.4 above, the photodissociation of $Zn(CH_3)_2$ molecules monolayered on a quartz substrate at room temperature gives only the slowly moving photofragments or the low-energy component signals, whilst photodissociation of the multilayered molecules gives not only a low-energy component but also a high-energy one. A similar dependence of kinetic energies on the surface coverage has been reported for the photodissociation of chlorine and CH_3Cl on silicon wafers.[8] The TOF distributions of chlorine photofragments are contrasted for thin and thick depositions of parent Cl_2 molecules on the substrate. The TOF distribution is bimodal for the thin-deposition case whilst it is unimodal and contains only a high-energy component for the thick-deposition case. The high-energy component of the photofragments originates from the topmost layer of multilayered Cl_2 and CH_3Cl molecules; hence the position of threshold appearance time is shifted toward longer time as the photon energy decreases. This is also the case for solid photodissociation of CH_2I_2 on Al_2O_3 and aluminum surfaces.[9] In the present experiment; the high-energy component in the TOF spectrum of Fig. 10(a) is asttributable to the direct dissociation of the topmost layer of $Zn(CH_3)_2$, viz.

$$CH_3ZnCH_3/\text{multilayer} + h\nu \rightarrow CH_3^{\cdot}\ (\text{fast}) \quad [3]$$

For the other compounds, $Sn(CH_3)_4$ and $In(CH_3)_3$, this direct photodissociation is observed as shown in the high-energy components of Figs 2(a) and 6. In the direct photodissociation process, the fastest CH_3 radicals can carry all the excess energy as the translational energy. The maximum translational energy is given by Eqn [4]:

$$E_T(\max) = h\nu - D_0 - \Delta E_{ads} \quad [4]$$

where ΔE_{ads} is the difference in adsorption energies of a parent molecule and of the $CH_3^{\cdot}$ radicals from the solid surface, and D_0 is the bond dissociation energy which is tabulated in Table 2. The adsorption energy is a function of adsorption geometry with atom(s) bonded to the solid surface and is typically a few kilojoules per mole. For the photodissociation of solid $Sn(CH_3)_4$, the threshold TOF corresponds to $360 \pm {}^{+80}_{-50}$ kJ mol^{-1}. This value gives $\Delta E_{ads} \approx 0$ using Eqn [4] with $h\nu = 619$ kJ and $D_0 = 250$ kJ mol^{-1}. ΔE_{ads} is expected to be close to zero in this case since $Sn(CH_3)_4$ is adsorbed by the $CH_3^{\cdot}$ attached to tin and the leaving species is a $CH_3^{\cdot}$ radical. For $In(CH_3)_3$, $\Delta E_{ads} = 110^{+80}_{-70}$ kJ mol^{-1} is obtained from the observed $E_{T(max)}$ of 310^{+80}_{-70} kJ mol^{-1} and $D_0 =$ 200 kJ mol^{-1}. ΔE_{ads} could be larger in this case because $In(CH_3)_3$ is adsorbed by interaction between the solid surface and the indium metal while the leaving $CH_3^{\cdot}$ radical can interact with the surface through its carbon or hydrogen atoms. For $Zn(CH_3)_2$, the observed maximum translational energy of the $CH_3^{\cdot}$ photofragment is 230^{+60}_{-40} kJ mol^{-1}, which is much lower than that of

Table 2 Thermodynamics of the decomposition of organometallic compounds

Reaction	ΔH (kJ mol^{-1})	Ref.
$Sn(CH_3)_4 \rightarrow Sn(CH_3)_3^{\cdot} + CH_3^{\cdot}$	251	23, 24
$Sn(CH_3)_2^{\cdot} + 2CH_3^{\cdot}$	498	23, 24
$Sn^{\cdot} + 4CH_3^{\cdot}$	907	23,24
$Ga(CH_3)_3 \rightarrow Ga(CH_3)_2^{\cdot} + CH_3^{\cdot}$	251	25
$In(CH_3)_3 \rightarrow In(CH_3)_2^{\cdot} + CH_3^{\cdot}$	197	25
$Zn(CH_3)_2 \rightarrow ZnCH_3^{\cdot} + CH_3^{\cdot}$	268	26

the other organometallics studied. This is presumably due to the large difference in adsorption energies, ΔE_{ads}, between $Zn(CH_3)_2$ and CH_3.

Tabares *et al.*[7] have observed a bimodal energy distribution in the photofragmentation processes of a multilayer of CH_3Br at 193 nm. They attribute this slow and wide distribution to the collision of CH_3 radicals within the deposit before the CH_3 fragments can emerge from the surface. This is possible because the optical depth of CH_3Br at 193 nm is 1200 nm. This seems, however, not to be the case in the present experiment because multilayered $Zn(CH_3)_2$ gives signals of both high- and low-energy components but monolayered $Zn(CH_3)_2$ yields only a low- and wide-energy component. The low-energy component appeared in the thin-deposition case of chlorine and CH_3Cl photodissociation.[8] This result suggests that the strong interaction between desorbates and substrate decelerates fragment velocity and also makes its distribution wide. Higashi[10] has stated in his report on photodissociation of monolayered $Al(CH_3)_3$ that the dissociative transition is not direct since so little energy is imparted to the ejected methyl radicals. This is consistent with the fact that subthermal desorption distributions have been observed in thermal desorption experiments.

Chuang and Domen[9] have explained that, in thick molecular layers, many of the photoexcited molecules beneath the surface may not dissociate because of repulsive interaction with the surrounding molecules as the molecular bond distance expands in these surrounding molecules. In addition, Bourdon *et al.*[6] have reported in their photodissociation of CH_3Br on a LiF substrate that the mean translational energy distribution of the photofragments is independent of the detction angle and, therefore, independent of the depth of the desorbing gas that is being traversed. This indicates that collisions between photofragments and desorbate are not important in the determination of the translational energy distribution.

4.2 Translational energy distributions of photofragments from solid phase photodissociation

The TOF spectra of the CH_3 photofragments from the organometallic compounds have rather wide peaks in the present experiment. The FWHM is as wide as 100 μs. This wide distribution reflects quick energy flow among the oscillators of solid molecules and the lattice mode of the substrate. Lin and his co-workers[20] have developed a theoretical model for the photodesorption using transition state theory. The energy of the activated complex is divided into two parts: vibrational and translational energies. The calculation of distribution in the translational energy E_T is essentially a problem of calculating the distribution of the vibrational energy among a collection of oscillators in the multilayered molecules. The vibrational energy of the activated complex along the reaction coordinate becomes a part of the translational energy of the dissociation products. In this case the translational energy distribution is given by Eqn [5]:

$$P(E_T) = 2\pi(1/\pi kT)^{3/2} E_T^{1/2} \exp(-E_T/kT) \quad [5]$$

Hence, T is a characteristic temperature of this distribution. We assume this equation is applicable to the photodissociation reaction on the substrate and in the solid phase. Figures 4, 5, 7 and 10 depict the translational energy distributions, $P(E_T)$, of CH_3 photofragments obtained from corresponding TOF spectra along with best-fit curves. Since two primary processes occur in the photodissociation as described above, a two-component fit is tested. The smooth curves through the experimental traces are fitted to composites of two Maxwell–Boltzmann distributions as given by Eqn [6]:

$$P(E_T) = \sum_{i=1}^{2} 2\pi(1/\pi kT_i)^{3/2} E_T^{1/2} \exp(-E_T/kT_i). \quad [6]$$

Calculated curves are fitted fairly well to the experimental results. Table 1 summarizes the results of average energies defined as $\bar{E}_{T_i} = (3/2)kT_i$.

Concerning the results of $Sn(CH_3)_4$, when one compares Fig. 4(b) with (c), the energy distribution above 8 kJ mol^{-1} in Fig. 3(b) is similar to that of Fig. 4(c), suggesting that at high laser energy flux, gas-phase photodissociation occurs. The low-energy components (average energy 2 kJ mol^{-1}) reflect surface photodissociation. This subthermal desorption is attributable to shallow potential wells for desorption.[21] The concept of what is occurring can be understood by performing an imaginary experiment of scattering molecules from surfaces and invoking microscopic reversibility. For shallow potential wells, high-energy incoming molecules can be imagined to

scatter with zero residence time. Low-energy molecules which scatter inelastically are easily trapped. In equilibrium, the flux-out is equal to the flux-in and therefore leads to a Maxwellian distribution. In photodesorption, however, only the molecules resident on the surface from prior trapping events contribute to the distribution. In this case the distribution cannot look Maxwellian if microscopic reversibility is to be satisfied. This concept explains the fact that Figs 4, 7 and 10 for CH_3 radicals from $Sn(CH_3)_4$, $In(CH_3)_3$ and $Zn(CH_3)_2$ do not completely fit to a Maxwellian distribution.

The parent molecule of $Sn(CH_3)_4$ is photodesorbed with comparatively large translational energy (~25 kJ mol^{-1}) as shown in Table 1. In the case of chlorine, it is rather small (~4 kJ mol^{-1}).[8] This difference may be attributable to the different nature of electronic states excited by laser irradiation. A Rydberg state can be excited for $Sn(CH_3)_4$ by 193 nm irradiation, whilst a valence state for chlorine. Repulsion forces between Rydberg orbitals ejects $Sn(CH_3)_4$ molecules from the surface because of the large diameters of Rydberg orbitals.

4.3 Photoejection of metals atoms

In the solid-phase photodissociation of $Sn(CH_3)_4$, Sn^+ signals are detected but these signals originate from dissociative ionization of photodesorbed parent molecules and not from photofragment tin metals, as described in Section 3.1.1 above. In fact, Table 1 shows that Sn^+ and $Sn(CH_3)_4^+$ have almost the same TOF thresholds (t_{TH}) and average energies (E_T). Tin metal atoms are not photodesorbed in our experimental conditions. Based on the ΔH values shown in Table 2, the formation of tin metal requires at least two photons at 193 nm and this process is reported to play a minor role compared with a one-photon process.[17] Higashi[10] has reported the absence of aluminum in his surface photodissociation of $Al(CH_3)_3$, suggesting that aluminum is strongly bound to the surface. The two-photon photolysis of $Ga(CH_3)_3$ adsorbed on a quartz plate has been studied at 243 nm by probing gallium atoms by laser-induced fluorescence (LIF).[12] When a gallium metal plate was irradiated by the same laser beam, no LIF signals were detected. This is also the case for $In(CH_3)_3$.[13] Thus, gallium and indium atoms originate from adsorbed $Ga(CH_3)_3$ and $In(CH_3)_3$, respectively. Photolysis of adsorbed $Zn(CH_3)_2$ on a quartz substrate gave, however, no LIF signals of zinc atoms.[13] It can be estimated from the Boltzmann energy distribution of the photofragment translational energy that the energy dissipation rate on a substrate is large. The atoms of the low-temperature-melting-point metals gallium and indium are photoejected, whilst the high-temperature-melting-point metals aluminum and zinc are not. By experimentally determining if metal atoms are photoejected, the nature of the bond between newly formed metal atoms and a substrate can be investigated.

4.4 Photodissociation of trimethylgallium

When $Ga(CH_3)_3$ is photodissociated in the solid phase (Fig. 8) CH_3 photofragments show a complicated TOF spectrum. This result suggests that the CH_3 radicals as generated from at least two processes, i.e. one from the parent molecule, $Ga(CH_3)_3$, and the other from a metastable molecular fragment, probably $GaCH_3$. Mitchell *et al.*[22] proposed that gas-phase photodissociation of $Ga(CH_3)_3$ at 222 nm produces $GaCH_3$. Since this species absorbs another UV photon, $GaCH_3$ photolysis acts as a 'bottleneck' in the production of a free gallium atom and also a CH_3 fragment. It is interesting to note that a similar situation pertains in the pyrolysis of $Ga(CH_3)_3$, where under certain conditions $GaCH_3$ remains as a polymer deposit after decomposition of $Ga(CH_3)_3$ and $Ga(CH_3)_2$.[14]

Acknowledgement M Kawasaki thanks the Cooperative Study Program of the Institute for Molecular Science. This work is partly supported by a Grant-in-Aid on Priority Area Research on 'Photo-excited process' supported by the Ministry of Education, Science, and Culture of Japan.

REFERENCES

1. Osgood, R M and Deutsch, T F *Science,* 1985, 227: 709
2. Yardley, J T *Laser Handbook* Bass, M and Stitch, M L (eds) Elsevier Science Publishers, Netherlands 1985
3. Hanabusa, M *Mat. Sci. Rep.*, 1987, 2: 51
4. Herman, I P *Chem. Rev.*, 1989, 89: 1323
5. Kawai, T and Sakata, T *Chem. Phys. Lett.*, 1980, 69: 33
6. Bourdon, E B D, Cowin, J P, Harrison, I, Polanyi, J C, Segner, J, Stanners, C D and Young, R A *J. Phys. Chem.*, 1984, 88: 6100
7. Tabares, F L, Marsh, E P, Bach, G A and Cowin, J P *J. Chem. Phys.*, 1987, 86: 738
8. Kawasaki, M, Sato, H and Nishi, N *J. Appl. Phys.*, 1988, 65: 792

9. Chuang, T J and Domen, K *J. Vac. Sci. Tech.*, 1987, A5: 473
10. Higashi, G S *J. Chem. Phys.*, 1988, 88: 422
11. Howitz, J S, Villa, E and Hsu, D S Y *J. Phys. Chem.*, 1990, 94: 7214
12. Suzuki, H, Mori, K, Kasatani, K, Kawasaki, M and Sato, H *J. Appl. Phys.*, 1988, 64: 371
13. Kawasaki, M, Kasatani, K, Sato, A and Nishi, N *Mat. Res. Soc. Sym. Proc.*, 1989, 129: 69
14. Shogen, S, Matsumi, Y, Kawasaki, M and Okabe, H *J. Appl. Phys.* (in press)
15. Shaw, P S, Sanchez, E, Wu, Z and Osgood, R M Jr *Chem. Phys. Lett.*, 1988, 151: 449
16. Thompson, H W *J. Chem. Soc.*, 1936: 108
17. Kawasaki, M and Sato, H *Laser Chem.*, 1987, 7: 109
18. Yu, C F, Youngs, F, Ysukiyama, K and Bersohn, R *J. Chem. Phys.*, 1986, 85: 1382
19. Nishi, N, Shinohara, H and Okuyama, T *J. Chem. Phys.*, 1984, 80: 3898
20. Lin, S H, Tsong, I S T, Ziv, A R, Szymonski, M and Loxton, C M *Physica Scripta*, 1983, T6: 106
21. Tully, J C *Surf. Sci.*, 1981, 111: 461
22. Mitchell, S A, Hackett, P A, Rayner, D M and Humphries, M R *J. Chem. Phys.*, 1985, 83: 5028
23. Lampe, F W and Niehaus, A *J. Chem. Phys.*, 1968, 49: 2949
24. Gedanken, A, Robin, M B and Kuebler, N A *J. Phys. Chem.*, 1982, 86: 4096
25. Kerr, J A *Chem. Rev.*, 1966, 66: 465
26. Jackson, R L *Chem. Phys. Lett.*, 1989, 163: 315